Sound radiation of a metaplate made of an acoustic black hole and local resonators

Jie Deng, Oriol Guasch, Laurent Maxit, Nansha Gao

inter.noise
21-24 AUGUST
SCOTTISH EVENT CAMPUS
GLASGOW
2022

Sound radiation of a metaplate made of an acoustic black hole and local resonators

Jie Deng[1]
School of Marine Science and Technology, Northwestern Polytechnical University
127# West Youyi Road, Xi'an, China

Oriol Guasch[2]
Department of Engineering, La Salle, Universitat Ramon Llull
C/Quatre Camins 30, 08022 Barcelona, Catalonia (Spain)

Laurent Maxit[3]
INSA–Lyon, Laboratoire Vibrations-Acoustique (LVA)
25 bis, av. Jean Capelle, F-69621 Villeurbanne Cedex, France

Nansha Gao[4]
School of Marine Science and Technology, Northwestern Polytechnical University
127# West Youyi Road, Xi'an, China

ABSTRACT

Acoustic black holes (ABHs) have not only proved very efficient in reducing vibrations in beams and plates at mid and high frequencies, but also in suppressing sound radiation. However, for lower frequencies with wavelengths larger than the ABH diameter waves cannot be trapped. It has been shown, though, that one can attach a periodic distribution of local resonators to the ABH plate and substantially diminish its vibration at low frequencies. Such design (local resonators plus ABH plate) can be viewed as a metaplate, referred to as the MMABH plate, with enhanced vibration properties as compared to a uniform plate or a standard ABH plate. In this work, we are interested in studying the radiation properties of the MMABH. Its sound power and radiation efficiency are characterized by means of a discretized radiation model and it is observed that broadband reduction in sound power level and far field radiated sound is attained. Non-negative intensity (NNI) also shows that sound reduction cannot be simply attributed to the damping effectivity of the ABH and resonators, but to the wave slowdown phenomenon inside the ABH that that breaks the coupling between bending and sound waves.

[1]dengjie@nwpu.edu.cn

[2]oriol.guasch@salle.url.edu

[3]laurent.maxit @insa-lyon.fr

[4]gaonansha@nwpu.edu.cn

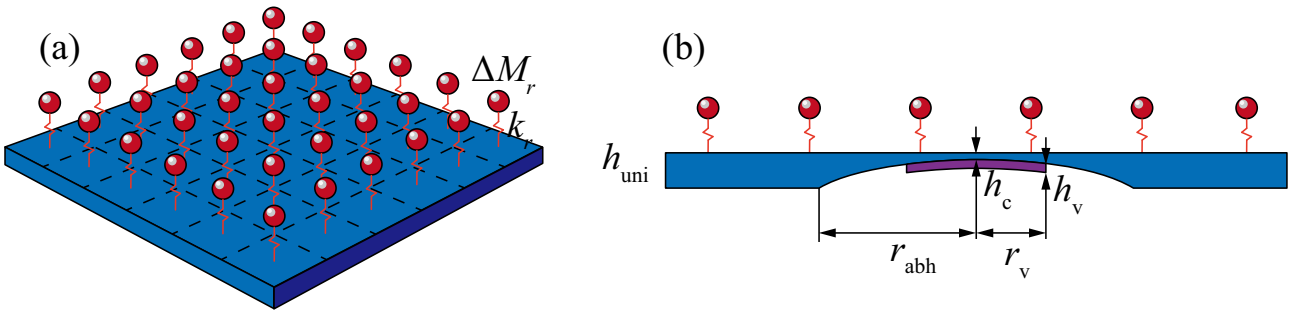

Figure 1: The geometrical model of the proposed MMABH metaplate: (a) 36 resonators attached to the plate surface, (b) thickness profile of the ABH plate.

1. INTRODUCTION

An ABH is usually achieved by diminishing the structural thickness of a beam or a plate following a power law profile [1]. Flexural waves entering the ABH slow down as the thickness diminishes while their amplitude augments. Vibration energy at the mid-high frequency range can be very effectively suppressed by placing a viscoelastic layer at the central region of the ABH [2]. While many works exist on ABH vibration reduction (see e.g., [3]), to date less research has been done on sound radiation. In [4], a plate with an array of 25 ABHs was numerically investigated. It was shown that improvement in sound radiation was not only due to vibration reduction but to notorious change in the dependence of the radiation efficiency with frequency. The later was further explained via wavenumber analysis [5, 6]. Moreover, transonic boundaries where flexural waves transition from supersonic to subsonic speed when slowing down inside the ABH were theoretically reported for flat plates in [7] and cylindrical shells in [8], and experimentally validated in [9].

Despite the effectiveness of ABHs concerning sound radiation is limited to mid and high frequencies, this has a profound impact in terms of transmission loss (TL) between dwellings because the typical drop of TL at the critical frequency can be suppressed [10, 11]. However, diminishing sound radiation of ABH plates at low frequencies remains a challenge even with new ABH designs [12, 13].

Some recent attempts to enhance the vibration performance of ABHs in the low frequency range have involved exploiting nonlinear effects [14, 15], the periodicity of tangled ABG cells [16], resorting to optimization strategies [17–20], or designing non-local ABH structures [21]. Another recent option proposed by the authors in [22] is that of attaching periodic local resonators to the ABH plate, following the key strategy of locally resonant metamaterials [23], in what we termed the MMABH plate. Usually, locally resonant metamaterials work in/near the frequency band where the resonators' eigen-frequencies belong, and have been proved useful for vibration reduction [24], sound insulation [25] and wave manipulation [26]. However, and in spite of some careful designs to expand their effective bandwidth [27], metamaterials perform well in a limited frequency range. In this sense, the MMABH metaplate in [22] constitutes a promising recourse to combine the effectiveness of periodic resonators at low frequencies with the efficacy of ABHs at high frequencies, to achieve broadband vibration reduction. That was studied in detail in [22] and in a companion paper in this conference. In this work, we will focus on the capability of the MMABH plate for broadband sound radiation reduction. We will do so by analyzing its sound power, radiation efficiency and non-negative intensity. The design of the MMABH is shown in Figure 1.

Table 1: Geometrical and material parameters of the ABH plate.

Geometry parameters	**Material parameters**
$m = 2.5$	$\rho_p = 7800$ kg/m^3
$L_x = 0.6$ m	$E_p = 210$ GPa
$L_y = 0.6$ m	$\eta_p = 0.01$
$h_{uni} = 0.01$ m	$\nu_p = 0.3$
$r_{abh} = 0.24$ m	
$\varepsilon = 0.3367$ m$^{-1.5}$	$\rho_v = 950$ kg/m^3
$h_c = 0.0005$ m	$E_v = 5$ GPa
$r_v = 0.24$ m	$\eta_v = 0.5$
$h_v = 0.0015$ m	$\nu_v = 0.3$

2. SOUND POWER LEVEL AND NON-NEGATIVE INTENSITY ANALYSIS

Following a Gaussian expansion method [28, 29], one can obtain the vibration velocity $\boldsymbol{v}$ on the MMABH plate surface after discretization [22]. The total radiated sound power can be expressed solely in terms of $\boldsymbol{v}$ and the radiation impedance, $\boldsymbol{Z}$, as (see e.g., [7, 8]),

$$W = \frac{\Delta S}{2}\mathrm{Re}\left(\boldsymbol{v}^{\mathrm{H}}\boldsymbol{p}\right) = \frac{\Delta S}{2}\mathrm{Re}\left(\boldsymbol{v}^{\mathrm{H}}\boldsymbol{Z}\boldsymbol{v}\right) = \boldsymbol{v}^{\mathrm{H}}\mathrm{Re}\left(\frac{\boldsymbol{Z}}{2}\right)\boldsymbol{v}\Delta S \equiv \boldsymbol{v}^{\mathrm{H}}\boldsymbol{R}\boldsymbol{v}\Delta S, \tag{1}$$

where ΔS represents the area of an elementary radiator. Note that in the last equality of Equation 1 we have introduced the resistance matrix, $\boldsymbol{R}$, which is real, symmetric and positive-definite. Besides, the radiation efficiency of the MMABH plate can be obtained from,

$$\sigma = \frac{W}{Z_0 N \Delta S \langle v^2 \rangle} = \frac{W}{\rho_0 c_0 \Delta S\, \boldsymbol{v}^{\mathrm{H}}\boldsymbol{v}}, \tag{2}$$

where $\langle v^2 \rangle$ stands for the mean square velocity (MSV) over the MMABH plate surface, Z_0 for the air acoustic specific impedance and N for the number of radiators.

On the other hand, to properly understand the radiation mechanisms of the MMABH plate it is also interesting to determine which portions of the plate contribute to the radiation of sound pressure at the far-field. One could resort to supersonic intensity or to non-negative intensity (NNI) [30] to that purpose. The second one has been chosen in this work. As suggested in [30], the NNI can be found with the help of an eigenvalue decomposition of the resistance matrix, $\boldsymbol{R}$. This provides the eigenvalue matrix $\boldsymbol{\Lambda}$ (diagonal) and the eigenvector matrix $\boldsymbol{\Psi}$ (normalized), with $\boldsymbol{\Psi}^\top\boldsymbol{\Psi} = \boldsymbol{I}$ and $\boldsymbol{\Psi}^\top\boldsymbol{R}\boldsymbol{\Psi} = \boldsymbol{\Lambda}$. Thus, we can re-express the resistance matrix as

$$\boldsymbol{R} = \boldsymbol{\Psi}\boldsymbol{\Lambda}\boldsymbol{\Psi}^\top = \boldsymbol{\Psi}\sqrt{\boldsymbol{\Lambda}}\sqrt{\boldsymbol{\Lambda}}\boldsymbol{\Psi}^\top = \boldsymbol{\Psi}\sqrt{\boldsymbol{\Lambda}}\left(\boldsymbol{\Psi}^\top\boldsymbol{\Psi}\right)\sqrt{\boldsymbol{\Lambda}}\boldsymbol{\Psi}^\top = \left(\boldsymbol{\Psi}\sqrt{\boldsymbol{\Lambda}}\boldsymbol{\Psi}^\top\right)\left(\boldsymbol{\Psi}\sqrt{\boldsymbol{\Lambda}}\boldsymbol{\Psi}^\top\right) \equiv \boldsymbol{\Phi}^\top\boldsymbol{\Phi}. \tag{3}$$

Equation 3 shows that the resistance matrix can be decomposed into two identical matrices. Here, $\boldsymbol{\Phi}$ can be treated as a mask that circumvents inactive radiators that do not contribute to the radiated sound power. The latter can be rewritten as

$$W = \boldsymbol{v}^{\mathrm{H}}\boldsymbol{R}\boldsymbol{v}\Delta S = \boldsymbol{v}^{\mathrm{H}}\boldsymbol{\Phi}^\top\boldsymbol{\Phi}\boldsymbol{v}\Delta S = \left(\boldsymbol{\Phi}\boldsymbol{v}\right)^{\mathrm{H}}\left(\boldsymbol{\Phi}\boldsymbol{v}\right)\Delta S \equiv \boldsymbol{\beta}^{\mathrm{H}}\boldsymbol{\beta}\Delta S. \tag{4}$$

In the last equality of Equation 4 we have defined the vector $\boldsymbol{\beta}$, whose entries, β_i, represent the square root of the NNI of each radiator. Bear in mind that the overall sound power remains the same provided

that one integrates the NNI over the whole surface. Finally, the NNI distribution can be computed from

$$\boldsymbol{I}_s^{\mathrm{NNI}} = \boldsymbol{\beta}^* \odot \boldsymbol{\beta}, \tag{5}$$

where $\odot$ symbolizes the Hadamard product (entrywise) and the superscript $*$ implies the complex conjugation operation.

3. NUMERICAL RESULTS

In the forthcoming simulations we consider the following design of an MMABH plate. First, we take an ABH plate with the geometrical and physical parameters listed in Table 1. Second, we distribute the surplus material ΔM =7.4494 kg extracted from the ABH indentation among 36 resonators, each one having mass $\Delta M_r = 0.2069$ kg, and link them to the ABH plate (see Figure 1). The first resonant frequency of the ABH plate is $f_1 = 128.5$ Hz and we tune the spring stiffness of the resonators to match their eigenfrequency with f_1. This results in $k_r = (2\pi f_1)^2 \Delta M_r = 31099$ N/m. The resonators have structural damping with loss factor $\eta_r = 0.2$.

The sound power level (SWL) of the three plates, MMABH, ABH and uniform (UNI) under a unit force excitation at $(0.5, 0.5)$ m is calculated according to Equation 1 and plotted in Figure 2a. As observed, the SWL of the ABH plate is considerably lower than that of the UNI plate above the ABH's cut-on frequency, $f_{\mathrm{cut-on}} = 428$ Hz, as reported in previous works [4, 7]. However, the ABH fails to reduce the SWL below $f_{\mathrm{cut-on}}$, especially at the first eigenfrequency of the ABH plate, $f_1 = 128.5$ Hz. The local resonators help fixing that problem as seen from the MMABH SWL curve in Figure 2a, where the peak at the ABH plate resonance disappears. If one compares the SWL of the three plates, the MMABH achieves notorious broadband reduction besides the other two. It behaves like the ABH plate above the cut-on frequency, but clearly overcomes it below. It also overcomes the UNI plate for the whole frequency range. Likewise, we have calculated the radiation efficiency of the three plates according to Equation 2, see Figure 2b. As known and seen in the figure, the radiation efficiency of the UNI plate has a maximum greater than 1 near the critical frequency, $f_{\mathrm{crit}} = 1172$ Hz. However, this is not the case for the ABH and the MMABH plates, thanks to the wave slowdown effect of the ABH profile. At low frequencies, between $f_1 = 128.5$ Hz and $f_{\mathrm{cut-on}} = 428$ Hz, the radiation efficiency of the MMABH plate is somewhat higher than that of the ABH plate. This is due to the low-frequency

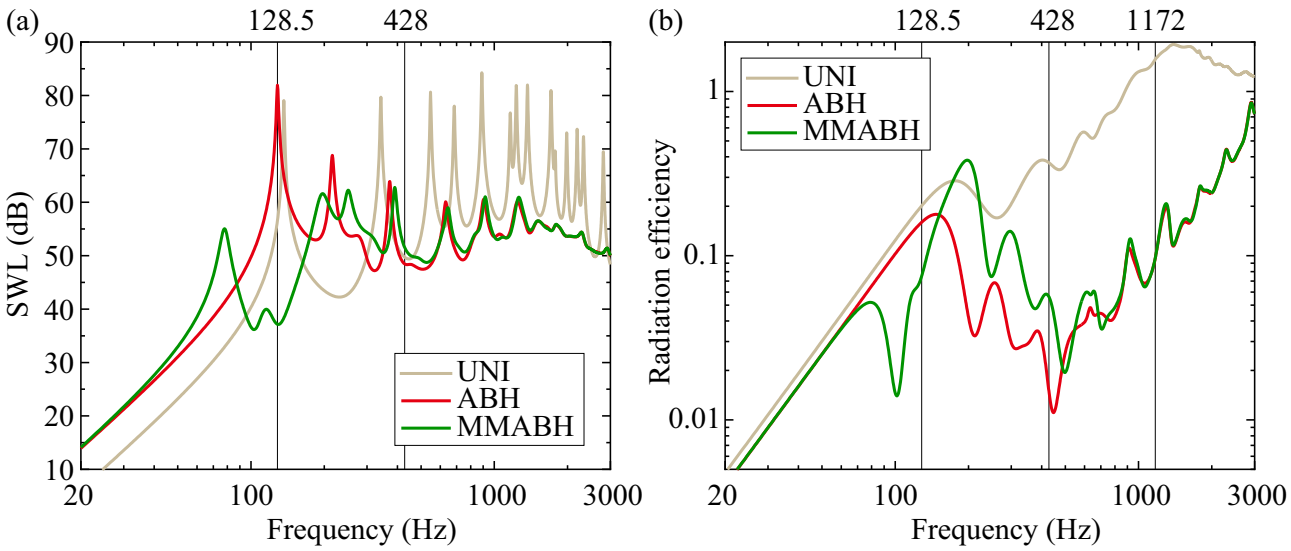

Figure 2: (a) Sound power level (SWL) and (b) radiation efficiency comparisons of the three plates.

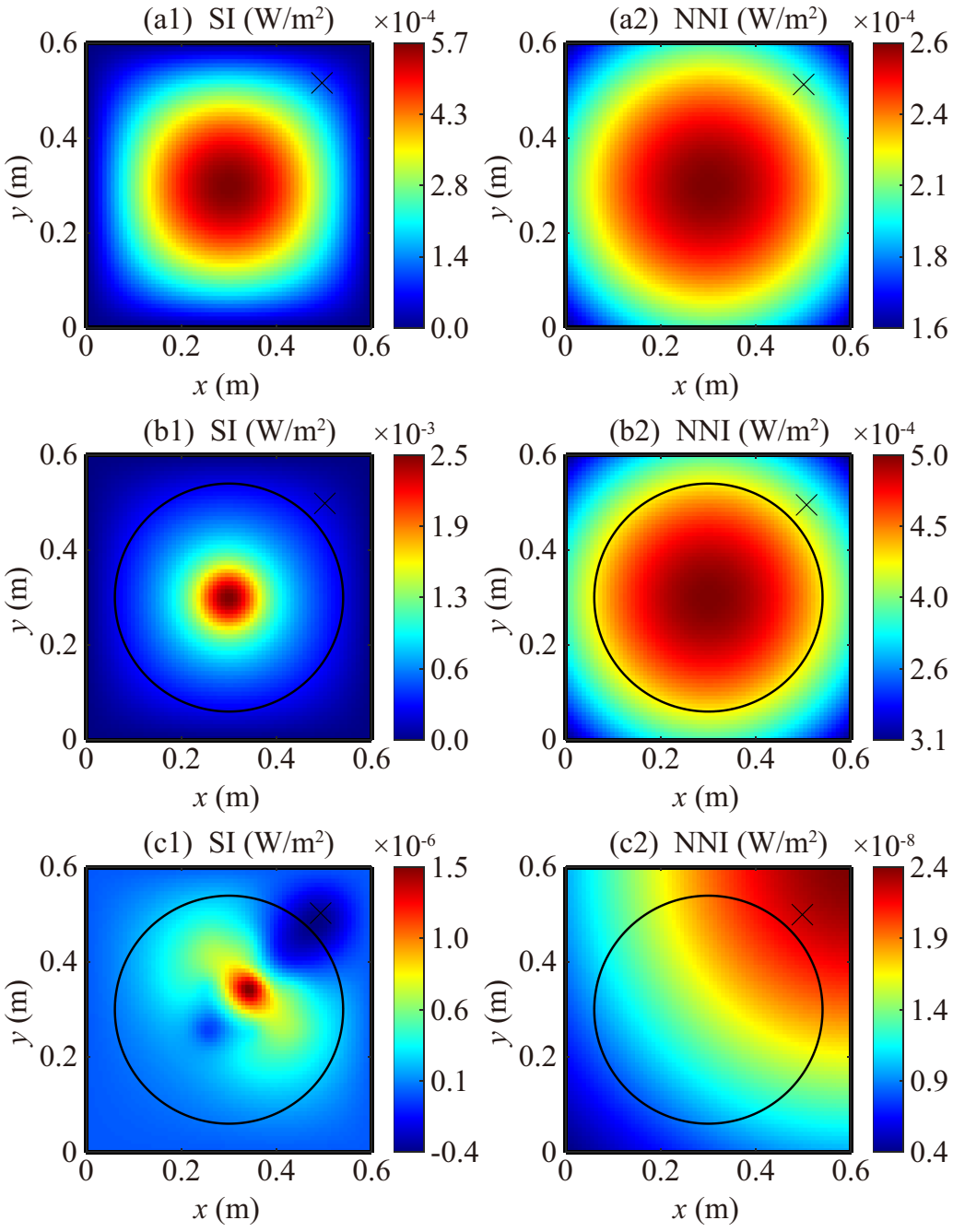

Figure 3: (a1)-(c1) The sound intensity (SI) for the uniform, ABH and MMABH plates, respectively. (a2)-(c2) The non-negative intensity (NNI) for the three plates. (a1)-(a2) correspond to the first resonant frequency 136.5 Hz, while (b1)-(b2) and (c1)-(c2) to 128.5 Hz. The black cross in each figure represents the point force.

coincidence effect that can be observed from dispersion curves (not shown here, see e.g., [25] for details).

To further understand the underlying mechanism for noise reduction at low frequencies, we next examine the NNI of the three plates. In the first column of Figure 3, we plot results for the sound intensity (SI) distribution, while in the second one we present plots for the NNI. The first row corresponds to the UNI plate, the second to the ABH one and the third to the MMABH plate. The results for the UNI plate are plotted at its first resonance peak, 136.5 Hz, while those of the ABH and MMABH correspond to the first resonance of the ABH plate, at 128.5 Hz. A first comparison between

the SI column and the NNI one shows that while the former has negligible values at the corners and edges of the plates, this is not the case for the NNI, indicating that these are also responsible for sound radiation (note that different scales have been used in the figures). However, the largest intensity values are located in the central region for the UNI and ABH plates. If we compare Figures 3a2 and 3b2, we can notice that the NNI of the ABH plate is higher than that of the UNI one, as also observed for the SWL peaks in Figure 2a. On the other hand, the SI and NNI distribution totally changes for the MMABH plate, the values being much smaller and, for the NNI, the maximum being close to the excitation point, see Figures 3c1 and 3c2. If ones looks at Figure 3c1, the sound intensity mainly locates in the ABH area. However, large negative intensity values are also appreciated indicating a strong recirculation region that does not radiate sound outwards. As said, the situation is totally different for the NNI plot, which tells us that the efficient radiation area is near the corner where the external force is applied (see Figure 3c2).

4. CONCLUSIONS

In this paper we have analyzed the sound radiation properties of a metaplate (MMABH) consisting of an ABH plate with a periodic distribution of structural damped local resonators. Such design has proved very effective in broadband vibration reduction and herein we have tested if that is also the case for noise radiation. We have shown that by tuning the eigenfrequencies of the resonators to the first resonance of the ABH plate, the MMABH plate performs as well as the former beyond the cut-on frequency but substantially improves its behavior in the low-frequency range. The comparison between the SWL of an MMABH, ABH and UNI plates shows that the former is clearly lower in the mean and at most individual frequencies. In addition, the radiation efficiency of the MMABH does not peak at the critical frequency as for a uniform plate, a result also found for a bare ABH plate. In fact the radiation efficiency of the MMABH is slightly higher than that of an ABH plate due to a low-frequency coincidence effect to be explained in more detail in future work. On the other hand, the analysis of the NNI on the MMABH surface at the first eigenfrequency of the ABH plate has shown how the MMABH plate only radiates in a region close to the excitation point, while the radiation area is located at the center of the indentation for the ABH plate. This is a direct effect of the locally attached resonators.

ACKNOWLEDGEMENTS

This work was supported by the National Natural Science Foundation of China (Grant No. 52171323) and the China Postdoctoral Science Foundation (Grant Nos. 2018M631194 and 2020T130533).

REFERENCES

[1] M.A. Mironov. Propagation of a flexural wave in a plate whose thickness decreases smoothly to zero in a finite interval. *Soviet Physics–Acoustics*, 34(3):318–319, 1988.

[2] Victor V Krylov. A new type of vibration damper based on flexural wave propagation in laminated wedges of power-law profile. *The Journal of the Acoustic Society of America*, 110(5):2654–2654, 2001.

[3] Adrien Pelat, François Gautier, Stephen C Conlon, and Fabio Semperlotti. The acoustic black hole: A review of theory and applications. *Journal of Sound and Vibration*, 476:115316, 2020.

[4] S.C. Conlon, J.B. Fahnline, and F. Semperlotti. Numerical analysis of the vibroacoustic properties of plates with embedded grids of acoustic black holes. *The Journal of the Acoustic Society of America*, 137(1):447–457, 2015.

[5] Xi Li and Qian Ding. Sound radiation of a beam with a wedge-shaped edge embedding acoustic black hole feature. *Journal of Sound and Vibration*, 439:287–299, 2019.

[6] Xiaodong Wang, Hongli Ji, Jinhao Qiu, and Li Cheng. Wavenumber domain analyses of vibro-acoustic decoupling and noise attenuation in a plate-cavity system enclosed by an acoustic black hole plate. *The Journal of the Acoustic Society of America*, 146(1):72–84, 2019.

[7] Li Ma and Li Cheng. Sound radiation and transonic boundaries of a plate with an acoustic black hole. *The Journal of the Acoustic Society of America*, 145(1):164–172, 2019.

[8] Jie Deng, Oriol Guasch, Laurent Maxit, and Ling Zheng. Annular acoustic black holes to reduce sound radiation from cylindrical shells. *Mechanical Systems and Signal Processing*, 158:107722, 2021.

[9] Li Ma and Li Cheng. Numerical and experimental benchmark solutions on vibration and sound radiation of an Acoustic Black Hole plate. *Applied Acoustics*, 163:107223, June 2020.

[10] Philip A Feurtado and Stephen C Conlon. Transmission loss of plates with embedded acoustic black holes. *The Journal of the Acoustic Society of America*, 142(3):1390–1398, 2017.

[11] Jie Deng, Oriol Guasch, Laurent Maxit, and Ling Zheng. Transmission loss of plates with multiple embedded acoustic black holes using statistical modal energy distribution analysis. *Mechanical Systems and Signal Processing*, 150:107262, 2021.

[12] Liling Tang and Li Cheng. Impaired sound radiation in plates with periodic tunneled Acoustic Black Holes. *Mechanical Systems and Signal Processing*, 135:106410, 2020.

[13] Jie Deng and Ling Zheng. Noise reduction via three types of acoustic black holes. *Mechanical Systems and Signal Processing*, 165:108323, 2022.

[14] Vitalyi E. Gusev, Chenyin Ni, Alexey Lomonosov, and Zhonghua Shen. Propagation of flexural waves in inhomogeneous plates exhibiting hysteretic nonlinearity: Nonlinear acoustic black holes. *Ultrasonics*, 61:126–135, 2015.

[15] Haiqin Li, Cyril Touzé, Adrien Pelat, François Gautier, and Xianren Kong. A vibro-impact acoustic black hole for passive damping of flexural beam vibrations. *Journal of Sound and Vibration*, 450:28–46, 2019.

[16] Liling Tang, Li Cheng, and Kean Chen. Complete sub-wavelength flexural wave band gaps in plates with periodic acoustic black holes. *Journal of Sound and Vibration*, 502:116102, 2021.

[17] Wei Huang, Chongcong Tao, Hongli Ji, and Jinhao Qiu. Enhancement of wave energy dissipation in two-dimensional acoustic black hole by simultaneous optimization of profile and damping layer. *Journal of Sound and Vibration*, 491:115764, 2021.

[18] Liling Tang and Li Cheng. Enhanced acoustic black hole effect in beams with a modified thickness profile and extended platform. *Journal of Sound and Vibration*, 391:116–126, 2017.

[19] Micah R Shepherd, Philip A Feurtado, and Stephen C Conlon. Multi-objective optimization of acoustic black hole vibration absorbers. *The Journal of the Acoustic Society of America*, 140(3):EL227–EL230, 2016.

[20] Meng-Xin He and Qian Ding. Data-driven optimization of the periodic beam with multiple acoustic black holes. *Journal of Sound and Vibration*, 493:115816, 2021.

[21] Siddharth Nair, Mehdi Jokar, and Fabio Semperlotti. Nonlocal acoustic black hole metastructures: Achieving broadband and low frequency passive vibration attenuation. *Mechanical Systems and Signal Processing*, 169:108716, 2022.

[22] Jie Deng, Oriol Guasch, Laurent Maxit, and Nansha Gao. A metamaterial consisting of an acoustic black hole plate with local resonators for broadband vibration reduction. *Journal of Sound and Vibration*, 526:116803, 2022.

[23] Zhengyou Liu, Xixiang Zhang, Yiwei Mao, Y. Y. Zhu, Zhiyu Yang, C. T. Chan, and Ping Sheng. Locally resonant sonic materials. *Science*, 289(5485):1734–1736, 2000.

[24] Penglin Gao, Alfonso Climente, José Sánchez-Dehesa, and Linzhi Wu. Single-phase metamaterial plates for broadband vibration suppression at low frequencies. *Journal of Sound and Vibration*, 444:108–126, 2019.

[25] N.G.R. de Melo Filho, L. Van Belle, C. Claeys, E. Deckers, and W. Desmet. Dynamic mass based sound transmission loss prediction of vibro-acoustic metamaterial double panels applied to the mass-air-mass resonance. *Journal of Sound and Vibration*, 442:28–44, 2019.

[26] Penglin Gao, Alfonso Climente, José Sánchez-Dehesa, and Linzhi Wu. Theoretical study of platonic crystals with periodically structured n-beam resonators. *Journal of Applied Physics*, 123(9):091707, 2018.

[27] D. Roca, J. Cante, O. Lloberas-Valls, T. Pàmies, and J. Oliver. Multiresonant layered acoustic metamaterial (mlam) solution for broadband low-frequency noise attenuation through double-peak sound transmission loss response. *Extreme Mechanics Letters*, 47:101368, 2021.

[28] Jie Deng, Ling Zheng, Pengyun Zeng, Yifang Zuo, and Oriol Guasch. Passive constrained viscoelastic layers to improve the efficiency of truncated acoustic black holes in beams. *Mechanical Systems and Signal Processing*, 118:461–476, 2019.

[29] Jie Deng, Ling Zheng, Oriol Guasch, Hang Wu, Pengyun Zeng, and Yifang Zuo. Gaussian expansion for the vibration analysis of plates with multiple acoustic black holes indentations. *Mechanical Systems and Signal Processing*, 131:317–334, 2019.

[30] Steffen Marburg, Eric Lösche, Herwig Peters, and Nicole Kessissoglou. Surface contributions to radiated sound power. *The Journal of the Acoustic Society of America*, 133(6):3700–3705, 2013.